Atmos. Chem. Phys. Discuss., https://doi.org/10.5194/acp-2017-537
Manuscript under review for journal Atmos. Chem. Phys.
Discussion started: 15 June 2017
© Author(s) 2017. CC BY 4.0 License.

Atmospheric Chemistry and Physics Discussions

Temporal variability of tidal and gravity waves during a record long 10 day continuous lidar sounding

Kathrin Baumgarten[1], Michael Gerding[1], Gerd Baumgarten[1], and Franz-Josef Lübken[1]

[1]Leibniz-Institute of Atmospheric Physics at the University of Rostock, Kühlungsborn, Germany

Correspondence to: Kathrin Baumgarten (k.baumgarten@iap-kborn.de)

Abstract.

Gravity waves (GW) as well as solar tides are a key driving mechanism for the circulation in the Earth's atmosphere. The propagation of gravity waves is strongly infected by tidal waves as they modulate the mean background wind field and vice versa, which is not yet fully understood and not implemented in many circulation models. The daylight capable Rayleigh-Mie-Raman (RMR) lidar at Kühlungsborn (54° N, 12° E) typically provides temperature data to investigate both wave phenomena during one full day or several consecutive days in the middle atmosphere between 30 and 75 km altitude. Outstanding weather conditions in May 2016 allowed for an unprecedented 10-day continuous lidar measurement which shows a large variability of gravity waves and tides on time scales of days. Using a 1-dimensional spectral filtering technique, gravity and tidal waves are separated according to their specific periods or vertical wavelengths, and their temporal evolution is studied. During the measurement a strong 24 h-wave occurs only between 40 and 60 km and vanishes after a few days. The disappearance is related to an enhancement of gravity waves with periods of 4-8 h. Wind data provided by ECMWF are used to analyze the meteorological situation at our site. The local wind structure changes during the observation period, which leads to different propagation conditions for gravity waves in the last days of the measurement and therefore a strong GW activity. The analysis indicates a further change in wave-wave interaction resulting in a minimum of the 24 h tide. The observed variability of tides and gravity waves on timescales of a few days clearly demonstrates the importance of continuous measurements with high temporal and spatial resolution to detect interaction phenomena, which can help to improve parametrization schemes of GW in general circulation models.

1 Introduction

The knowledge of atmospheric waves is crucial for our understanding of the circulation in the Earth's atmosphere. The propagation of different waves, e.g., gravity and tidal waves, and their interaction is a vital geophysical process, which couples the different atmospheric layers due to the transport of momentum and energy. Gravity waves (GW) and tides differ in their sources. While gravity waves are mostly generated in the troposphere/lower stratosphere through the flow above orographic structures, convective instabilities, wind shears, jet streams or wave-wave interactions, tides are excited by solar heating of water vapor in the troposphere, ozone in the stratosphere and mesopause region as well as oxygen above 90 km altitude (Chapman and Lindzen, 1970; Forbes, 1984; Fritts and Alexander, 2003). Due to the excitation process tides have periods of one solar day

Atmos. Chem. Phys. Discuss., https://doi.org/10.5194/acp-2017-537
Manuscript under review for journal Atmos. Chem. Phys.
Discussion started: 15 June 2017
© Author(s) 2017. CC BY 4.0 License.

Atmospheric Chemistry and Physics Discussions

(24 h) and its harmonics like 12 h or 8 h. The tidal propagation can be either Sun-synchronous or not, and therefore tides are called migrating or non-migrating tides (Forbes, 1995). They modulate the background wind field together with planetary waves and therefore have an impact on the propagation conditions for gravity waves (e.g., Eckermann and Marks, 1996; Senf and Achatz, 2011). Upward propagating GW transport energy and momentum and deposit them during their breaking and filtering to the mean background flow (Holton and Alexander, 2000; Fritts and Alexander, 2003). Models typically use only simplified parametrizations of gravity wave drag resulting in larger discrepancies between model and measurement data (e.g., Kim et al., 2003). Therefore, additional data are required for validation and more observational data are necessary for improving these parametrizations (Geller et al., 2013).

The middle atmosphere is one of the key regions for the interaction of gravity waves and tides. To investigate both wave phenomena different satellite and ground-based techniques (lidar, radar, radiosondes, rocket soundings, and airglow measurements) were developed within the last decades (e.g., Gille et al., 2008; Hertzog et al., 2008; Preusse et al., 2008). Satellite data give an global overview of GW and tides. For instance, the climatology of tides in the MLT region has been revealed by temperature/wind observations such as the High Resolution Doppler Interferometer (HRDI), Wind Imaging Interferometer (WINDII) and the Microwave Limb Sounder (MLS) on board of the UARS satellite, or the TIMED Doppler Interferometer (TIDI) and the Sounding of the Atmosphere using Broadband Emission Radiometry (SABER) instrument on board of the TIMED satellite (e.g., Sakazaki et al., 2012). However, satellites need a large time interval of typically several weeks to cover 24 h of local time. Consequently, any short-term variability in the dynamic features gets lost. Radar measurements of horizontal winds produce nearly continuous data sets, from which the short-term variability of gravity and tidal waves can be investigated, but only in a limited altitude range of approximately 70-100 km (Hoffmann et al., 2010). To cover the entire middle atmosphere the lidar is the only measurement technique which provides temperature data from the troposphere/lower stratosphere to the mesopause region or even higher with a suitable temporal and vertical resolution to resolve the short-term variability. Lidar data provide vertical information of the atmospheric parameters over time at the particular location. The Rayleigh-Mie-Raman (RMR) lidar located at Kühlungsborn is able to provide these information up to 75 km altitude under nighttime as well as under daytime conditions (Gerding et al., 2013, 2015, 2016; Kopp et al., 2015), while other lidar instruments cover only a small altitude range and/or they measure only during nighttime conditions (Gardner and Voelz, 1987; Chu et al., 2011; Wilson et al., 1991).

This paper presents main features of wave activity at mid-latitudes for an altitude range from the lower stratosphere to the upper mesosphere on short time scales of 10 days in May 2016. To our knowledge, this is the longest continuous data set retrieved by a RMR lidar. The daylight capability of the Kühlungsborn RMR lidar as well as exceptionally good weather conditions make it possible to investigate wave structures over this time period, which allows to study the short-term variability of gravity waves and tides. The lidar data is analyzed in spatial domain on the one hand and in time domain on the other hand to distinguish between different waves either because of their vertical wavelengths or their periods. Data from the European Centre for Medium-Range Weather Forecasts (ECMWF) are used to characterize the background conditions in the troposphere and stratosphere based on hourly high-resolution forecasts (cycle 41r2 TCO1279/O1280). The organization of this paper is as follows. In Section 2 we describe our lidar instrument and how the data are treated. Section 3 presents the available temperature data during the 10 days and their related temperature deviations. In Section 4 we present the short-term variation of the gravity

© Author(s) 2017. CC BY 4.0 License.

wave activity as well as the tidal activity. In addition to the lidar data, ECMWF data are used in Section 5 to characterize the background state of the atmosphere. The results are discussed in Section 6. Finally, the results are summarized and a conclusion is given in Section 7.

2 Instrumental Setup and Data

The Rayleigh-Mie-Raman lidar at Kühlungsborn was developed in 2009/2010 (Gerding et al., 2016). The transmitter mainly consists of a flash lamp pumped, injection-seeded Nd:YAG laser. We use the second harmonic of the laser output at 532 nm as emission wavelength due to a better signal-to-noise ratio compared to the fundamental laser output at 1064 nm. To measure during daytime, special spatial and spectral filtering techniques are used to suppress the solar background during the day. As a prerequisite for these techniques, the seeder is locked to an iodine absorption line for achieving high frequency stability and the laser beam divergence is reduced to ∼50 µrad using a 10x beam widening telescope. Afterward, the beam is guided co-axially with the receiving telescope into the atmosphere. The field of view (FOV) of the receiver is limited by a fiber cable with a small core diameter of 0.2 mm, resulting in a small field of view of only 62 µrad. The advantage is a reduction of the scattered background light from the Sun. A narrow band interference filter (IF) as well as two Fabry-Pérot-etalons (FPE) are used for spectral filtering. The IF has a full-width-at-half-maximum (FWHM) of about 130 pm. The etalons have a free spectral range (FSR) of about 120 pm (140 pm) and a FWHM of about 4 pm (4.5 pm), respectively. The FWHM of the etalons is on the order of the Doppler-width of the backscattered Rayleigh signal. This means that a small part of the backscattered Rayleigh signal is blocked depending on the actual Doppler-width of the backscattered light, thus, it depends on the atmospheric temperature at the particular scattering altitude. The reduced signal is not proportional to the atmospheric density anymore and therefore the classical retrieval for temperature is not valid. To overcome this issue, an altitude dependent transmission correction is applied for calculating absolute temperatures. Further information about the correction scheme and the validation can be found in Gerding et al. (2016).

To reduce the effects of tropospheric turbulence on the laser beam propagation and the alignment of laser and telescope FOV, an active beam-stabilization based on a Piezo-coupled mirror is used (Eixmann et al., 2015). Absolute temperatures are retrieved by integration of the range corrected backscattered signal assuming hydrostatic equilibrium (Hauchecorne and Chanin, 1980). The initial temperature value for integration is taken from CIRA-86 (Fleming et al., 1990) in an altitude range between 70 and 75 km for the whole day due to the strong solar background at the Sun's maximum. The temperatures become independent from the start temperature approximately one scale height below the selected altitude of this temperature. The integration time to retrieve the temperatures is 2 h with a temporal shift of 15 min. The vertical resolution is 1 km. Due to additional aerosol scattering below 30 km only temperatures above this altitude are taken into account in this paper.

To investigate different waves, temperature deviations from a slowly varying background field are determined. These deviations are retrieved by a subtraction of a mean temperature and by filtering in spatial and temporal domain using a Butterworth filter of fifth order. The filtering allows to distinguish between different wave components. A further description of the method

Atmos. Chem. Phys. Discuss., https://doi.org/10.5194/acp-2017-537
Manuscript under review for journal Atmos. Chem. Phys.
Discussion started: 15 June 2017
© Author(s) 2017. CC BY 4.0 License.

Atmospheric Chemistry and Physics Discussions

can be found in Baumgarten et al. (2017). In addition, a composite analysis of the lidar data as described in Kopp et al. (2015) is used to investigate mean amplitudes of tidal waves.

3 Temperatures and temperature deviations

Temperatures from 4 May 07:45 UT to 13 May 2016 23:45 UT are shown in Figure 1 for an altitude range of 30 to 70 km. The highest temperatures of up to 280 K occur in the stratopause region (∼50 km). There is a large variation present around the stratopause region which is due to atmospheric waves. These variations are mainly caused by tidal waves as the observed periods are close to one solar day (24 h). This feature is weaker at the end of the 10 day period. To highlight the wave structures,

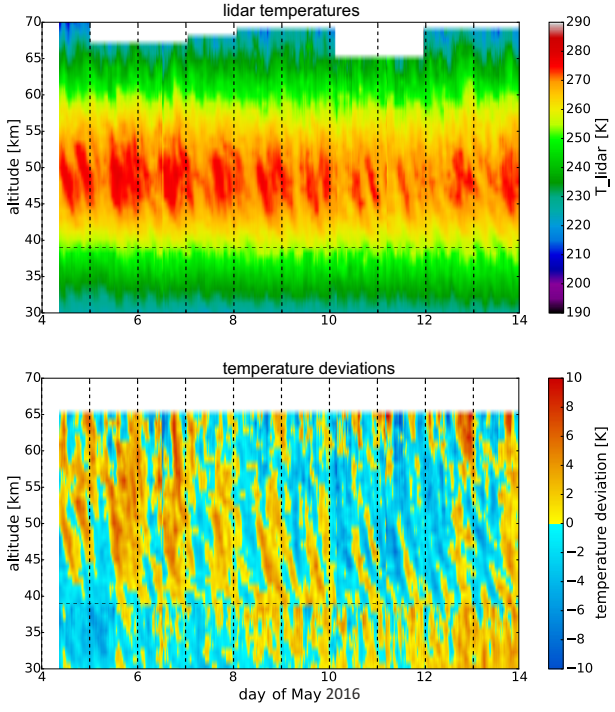

Figure 1. Temperature observed by the RMR lidar at Kühlungsborn on 4 - 13 May 2016 (at the top) and the temperature deviations from a mean temperature (at the bottom). The horizontal dashed line indicates the transition height between different receiver channels.

temperature deviations from a mean temperature profile over the entire days are calculated. They are also shown in Figure 1. The overall variation seems to be dominated by a modulation of several days presumably caused by a planetary wave resulting in increasing temperatures with time below 40 km and decreasing temperatures above. Furthermore, this large scale variation is superimposed by dominant waves with periods of 24 h (e.g. 5 - 8 May) as well as various other waves. In general, these exceptional long data set does not only contain tidal waves, also gravity waves as well as large scale waves presumably caused by planetary waves with periods of several days are visible.

Atmos. Chem. Phys. Discuss., https://doi.org/10.5194/acp-2017-537
Manuscript under review for journal Atmos. Chem. Phys.
Discussion started: 15 June 2017
© Author(s) 2017. CC BY 4.0 License.

Atmospheric Chemistry and Physics Discussions

To resolve the range of periods, which are occurring, the power spectral density is calculated using as a Lomb-Scargle periodogram. The result is shown in Figure 2 in terms of frequency with an additional period scale. As already seen from the temperature deviations from a mean profile, different waves superimpose in the time series above our site. During the measurement a 24 h wave component is dominating the temperature deviations, but also waves with smaller periods of 5, 8, 12 h can be seen. For comparison, the expected slope of gravity waves of $-\frac{5}{3}$ is shown, which was found to be universal (VanZandt, 1982). In addition to gravity and tidal waves, also waves on planetary scales with periods of 48 and larger than 100 h are observed.

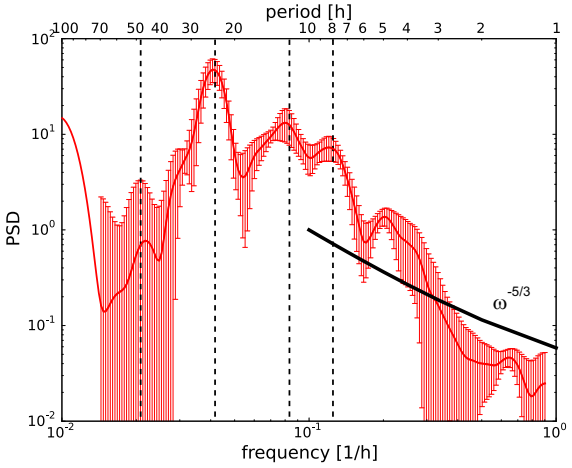

Figure 2. Smoothed power spectral density (PSD) as a function of frequency on 4 - 13 May 2016 calculated from the temperature deviations from a mean at 50 km altitude. The vertical dashed lines indicate periods of 8, 12, 24, and 48 h. The error bars denote the standard deviation of the power spectral density calculated from spectra obtained during the first and the second half of the measurement and the spectra for the whole measurement.

To analyze the variability of the waves further, a separation between different wave types has to be made. A 1-dimensional Butterworth filter is applied to extract temperature deviations induced by gravity waves. The cut off wavelength/period is 15 km/8 h, respectively, due to the assumption that tides have larger vertical wavelengths and periods. The resulting temperature deviations are shown in Figure 3 for vertically and temporally filtered data. While the vertical filtering leads to wave structures with relatively small vertical wavelengths ($\lambda_z < 15$ km), the temporal filtering method extracts only waves with periods smaller than 8 h and typically larger vertical wavelengths. The direct comparison of these two data sets shows differences in the regularity of the wave structures over the whole altitude range. Throughout the measurement time the wave structures in the temporally filtered data (lower panel) seems much more coherent than those of the vertically filtered data (upper panel). Especially in an altitude range below 40 km and above 55 km the structures from the vertically filtered data look more perturbed. Within this altitude range clear waves can be identified in most of the time. In the last few days the amplitude of the temperature deviations is increasing, especially on the 10-11 May. This indicates different propagation conditions for these waves which is further investigated in the next section. To calculate the temperature variations that are induced by tides, the Butterworth filter

Atmos. Chem. Phys. Discuss., https://doi.org/10.5194/acp-2017-537
Manuscript under review for journal Atmos. Chem. Phys.
Discussion started: 15 June 2017
© Author(s) 2017. CC BY 4.0 License.

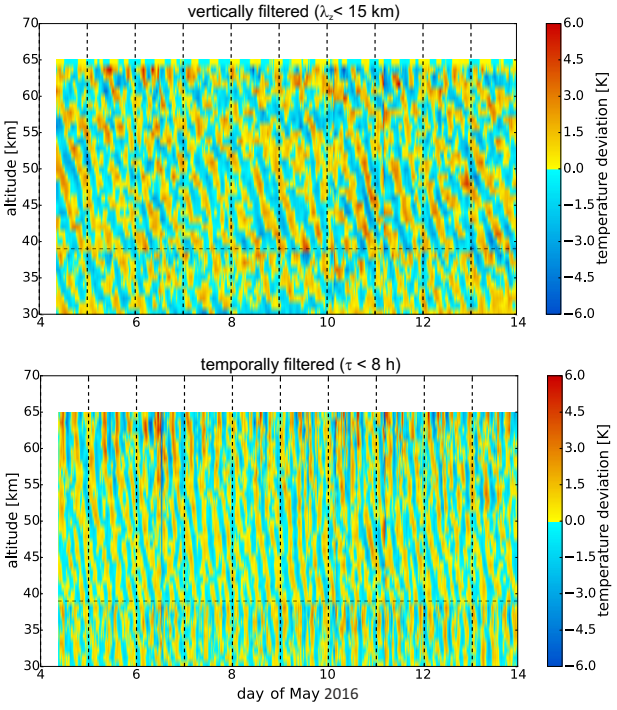

Figure 3. Temperature deviations for the vertically filtered (at the top) and the temporally filtered data (at the bottom) on 4 - 13 May 2016. The horizontal dashed line indicates the transition height between different receiver channels.

is used as a low pass filter with the same cut off parameters as for the gravity waves (not shown here). The variability of the different waves is shown in the next section.

4 Tidal and gravity wave variability

The variability of the waves observed is quantitatively investigated by using a wavelet transformation to calculate the periods of these longer and shorter scale waves. This is done by applying a Morlet wavelet of the fifth order to the filtered temperature deviations for a specific altitude. The temporal evolution of the periods is separately calculated for tides and gravity waves and is shown in the next two subsections.

4.1 Tidal variability

The wavelet spectra in three different altitudes for the so called tidal observations are shown in Figure 4 for the vertically (left) and for the temporally filtered data (right). In the beginning and in the end of the measurement the wave amplitudes are over- or underestimated due to edge effects and are therefore not taken into account. The boundary to this so-called cone of influence is denoted by the white curved line. At the lowest altitude of 40 km the vertically filtered data contain waves with periods between

Atmos. Chem. Phys. Discuss., https://doi.org/10.5194/acp-2017-537
Manuscript under review for journal Atmos. Chem. Phys.
Discussion started: 15 June 2017
© Author(s) 2017. CC BY 4.0 License.

Atmospheric Chemistry and Physics Discussions

6 and 24 h with only small amplitudes of about 1 K. While the wave with a period of 24 h is visible over the whole sounding, other wave components occur more sporadically. For example, the vertically filtered data show that there are less waves with

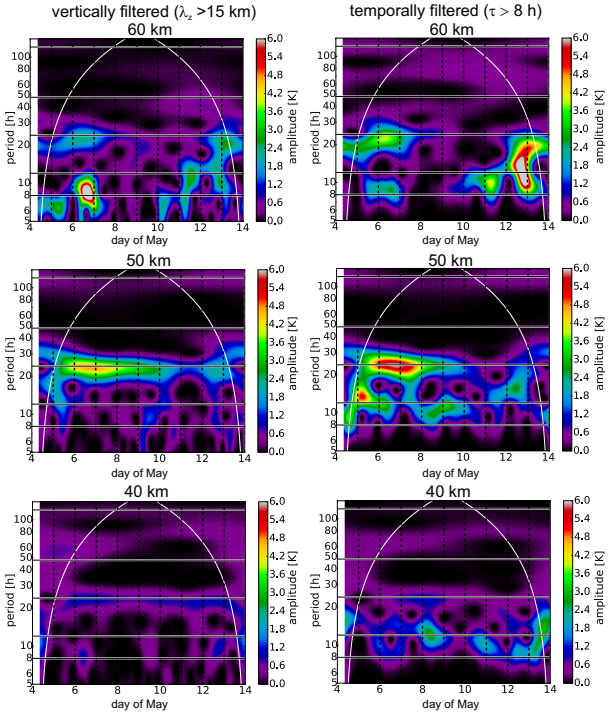

Figure 4. Wavelet spectrum for periods of larger scale waves calculated from vertically (left) and temporally filtered data (right) on 4 - 13 May 2016 at an altitude of 40 km (at the bottom), 50 km (in the middle) and 60 km (at the top). The horizontal lines indicates periods with 8, 12, 24, 48 and 120 h. The white curved line shows the edge of the cone of influence.

periods between 6 and 14 h and vertical wavelengths of more than 15 km, while there is already a higher activity of waves with periods from 8 to 24 h from the temporally filtered data. This indicates that especially the semidiurnal and the terdiurnal wave components are differently represented in the vertically and in the temporally filtered data. As a result this means either these tidal components have smaller vertical wavelengths as assumed or the most occurring waves in this period range are related to gravity waves.

At 50 km altitude the wave activity of especially the diurnal component is increased in the vertically filtered data as well as in the temporally filtered data. The first one shows amplitudes of 4 K for this component with the strongest occurrence on the 6 - 7 May 2016. Later this component becomes weaker. This behavior is even more pronounced in the temporally filtered data, where amplitudes of up to 6 K arise for the diurnal component in the first days. The amplitudes decrease to less than 1.5 K between the 10 May and the end of the measurement period. Other components with periods between 8 and 12 - 13 h are also visible, but they reveal smaller amplitudes and are less persistent compared to the diurnal component. The unexpected decrease of the diurnal component shown above indicates a strong short-term variability for tidal components, which are often referred

Atmos. Chem. Phys. Discuss., https://doi.org/10.5194/acp-2017-537
Manuscript under review for journal Atmos. Chem. Phys.
Discussion started: 15 June 2017
© Author(s) 2017. CC BY 4.0 License.

Atmospheric Chemistry and Physics Discussions

Table 1. Time intervals in May 2016 for the composite analysis and the related number of days and measurement hours during each interval.

Interval	no. of days	duration [h]	representation in Figure 5
01-09 May	7	161.3	dashed line
10-28 May	7	113.4	dotted line
01-28 May	14	274.7	solid line

to be constant (e.g. from the satellite community). At an altitude of 60 km this intermittency of the tidal signature becomes even stronger. The diurnal component completely vanishes after the 9 May 2016 for the vertically filtered as well as for the temporally filtered data and shows again a slight increase after the 12 May.

Especially the temporally filtered data do not solely contain tidal wave structures, instead there are also other longer periodic gravity waves included. To be sure that the potential bias caused by gravity waves is small, we also calculated the mean tidal amplitudes for the diurnal, semi- and terdiurnal component over three time intervals within May 2016. The number of days included in these intervals is given in Table 1. The calculation is based on the overlaying of temperature data for each of the days within the selected interval (Kopp et al., 2015). This composite of data is fitted with an harmonic function of fixed periods according to the solar tides. The mean amplitudes of the tidal components in each interval are shown in Figure 5. The monthly mean amplitude (solid line) of the semi- and terdiurnal tide does not show a relevant increase with altitude between 30 and 70 km. Only the diurnal component shows an increase of the amplitude up to 2 K at an altitude of 50 km. Above, the amplitude decreases again and reaches a value of 1 K at 60 km altitude. In comparison to this, the amplitude of the semidiurnal component varies only between 0.5 and 1 K. The amplitudes of the terdiurnal component are smaller than 0.5 K and they are therefore negligible compared to gravity waves with much larger amplitudes.

A closer look to the single time intervals reveals huge differences in the amplitudes of the diurnal component over the month, especially above 43 km altitude. The small variability below this altitude indicates a constant excitation over the whole time period, otherwise the differences mentioned before would also occur in this altitude range. The results from the wavelet analysis for the diurnal wave component at an altitude of 40 km also supports this statement (see Figure 4 at the bottom). Above 43 km the amplitude of the diurnal tide is significantly larger in the first interval as in the monthly mean. This is not visible for the other tidal components. Here the amplitudes are partly larger in the first time interval, at other altitudes in the second time interval. On the contrary, the amplitude of the diurnal component is constantly smaller in the last days of May than in the mean. The differences of the amplitudes during the different intervals are about 50% of the absolute value. The results for the diurnal component are in agreement with the temporal evolution of this component in the wavelet analysis, besides the slightly different amplitudes. The origin of these differences in the amplitudes lies in the filtering methods, which are not exclusively restricted to tides, also other long periodic waves are included in the data. Additionally to this, some long periodic gravity waves which could be Doppler shifted to periods larger than the Coriolis period may also be included. These waves would lead to higher amplitudes in the results from the wavelet analysis compared to those from the composite analysis. To

Atmos. Chem. Phys. Discuss., https://doi.org/10.5194/acp-2017-537
Manuscript under review for journal Atmos. Chem. Phys.
Discussion started: 15 June 2017
© Author(s) 2017. CC BY 4.0 License.

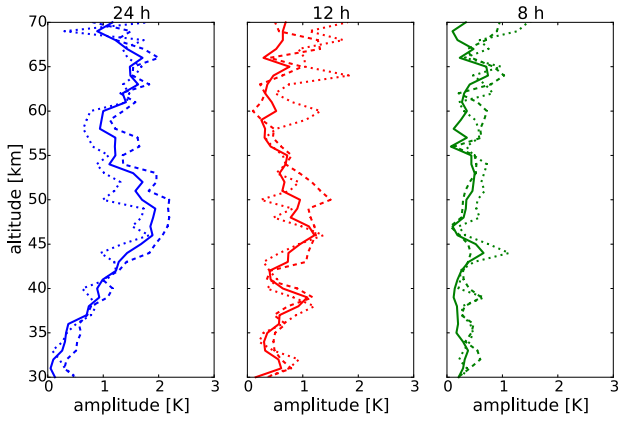

Figure 5. Tidal amplitudes for the diurnal (left), the semidiurnal (in the middle) and the terdiurnal (right) component derived from a composite analysis during 14 measurement days in May 2016 (solid line), the first days of May (dashed line) and the last days of May (dotted line). A definition of the time intervals is given in Table 1.

summarize this, the amplitudes of tides vary with time, but differently for different altitudes. They may increase at a certain altitude without a corresponding enhancement at other altitudes.

4.2 Gravity wave variability

As a comparison the same analysis is done for temperature deviations induced by gravity waves. The calculated wavelet spectra for the same altitudes are shown in Figure 6. The periods look quite different than for the tidal wave features shown in Figure 4. The dominant periods are much smaller than 24 h in most of the time and at every altitude between 40 and 60 km, even if the filtering was done with respect to vertical wavelengths. For the temporally filtered data this is per construction due to the cut off period. At 40 km altitude waves with periods between 6 and 12 h are observed from the vertically filtered data with amplitudes of up to 3 K on several days during the sounding. The largest amplitudes are observed for waves with periods of about 10-12 h. The temporally filtered data reveal lower amplitudes of about 0.5-1.5 K of waves with periods smaller than 8 h. At an altitude of 50 km the wavelet amplitudes are slightly reduced and large amplitudes occur more sporadically. On 10/11 May a wave with a period of 8 h becomes strong for the vertically filtered data. The appearance of this wave is even more pronounced at 45 km altitude (later shown in section 5). The temporally filtered data also show such a wave signature, but with a reduced amplitude due to the cut off period of 8 h. The GW signatures from the vertically filtered data are less pronounced above an altitude of 60 km, except for the signature on the 10 May. As seen before, a strong diurnal component is visible for the tidal wave features. This feature decreases at the same time when the gravity waves with a period around 8 h become important. Both phenomena are reduced above the stratopause. Therefore, we assume that the disappearance of the diurnal tidal component and these gravity waves is related to a wave-wave or wave-mean flow interaction between these two kinds of waves. To understand this behavior, it is necessary to investigate the mean background state of the atmosphere. This is done in the next Section with the use of ECMWF data of the integrated forecast system (cycle 41r2).

Atmos. Chem. Phys. Discuss., https://doi.org/10.5194/acp-2017-537
Manuscript under review for journal Atmos. Chem. Phys.
Discussion started: 15 June 2017
© Author(s) 2017. CC BY 4.0 License.

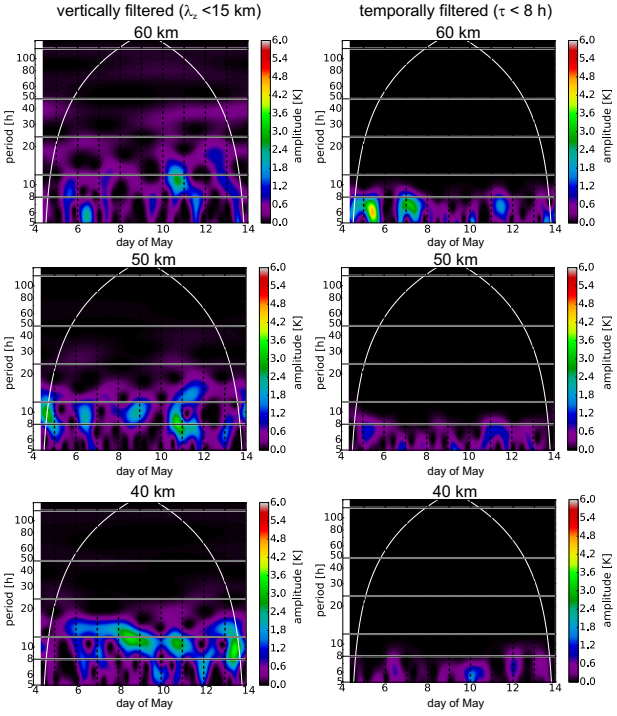

Figure 6. Wavelet spectrum for periods of gravity waves calculated from vertically (left) and temporally filtered data (right) on 4 - 13 May 2016 at an altitude of 40 (at the bottom), 50 (in the middle) and 60 km (at the top). The horizontal lines indicates periods with 8, 12, 24, 48 and 120 h. The white curved line shows the edge of the cone of influence.

5 Meteorological situation

The propagation of tidal and gravity waves depends on wind conditions as well as on their interaction. A change in the excitation of tidal waves could also lead to temporal differences in these waves (e.g., Achatz et al., 2008). ECMWF data provide temperature, ozone and horizontal wind information. The data above Kühlungsborn are studied to reveal if there were changes during the sounding period. The temperature data provided by ECMWF is shown in Figure 7 to make sure that ECMWF is able to produce overall reliable results of the meteorological situation above Kühlungsborn. Therefore, ECMWF temperatures and the temperature deviations from a mean temperature profile are shown for the same altitude range as the lidar data.

In general, the comparison to the lidar data (Fig. 1) shows similar structures. ECMWF temperature deviations from a mean reveal also strong wave structures with periods of 12 and 24 h. Especially in the altitude range between 40 and 50 km the phases of the wave structures are very similar to the lidar temperature deviations (see Fig. 1 at the lower panel). But for higher altitudes the similarity gets lost as ECMWF shows a wave structure with a much longer period compared to the lidar data. In the altitude range between 30 and 40 km smaller differences between the lidar and the ECMWF data are present, e.g., the tilt of the phase

Atmos. Chem. Phys. Discuss., https://doi.org/10.5194/acp-2017-537
Manuscript under review for journal Atmos. Chem. Phys.
Discussion started: 15 June 2017
© Author(s) 2017. CC BY 4.0 License.

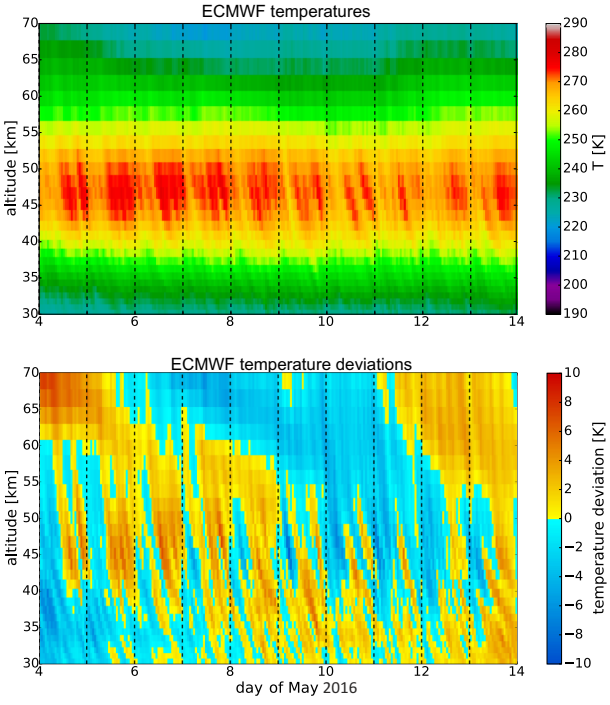

Figure 7. Temperature provided by the integrated forecast system of ECMWF (cycle 41r2) extracted with 1 hour temporal resolution on 4 - 13 May 2016 (at the top) and the calculated temperature deviations from the mean temperature (at the bottom).

lines differs among these two data sets. But the overall wave structures, especially for tidal waves with periods of 12 h and 24 h, are similar up to an altitude of 50 km, while shorter periodic wave structures are different in both data sets. However, ECMWF data provide useful information at least of the background atmosphere and are suitable to get a comprehensive understanding of the state of the atmosphere.

The overall zonal and meridional wind above Kühlungsborn derived from ECMWF is studied to reveal if there are changes for the propagation conditions of the waves. Therefore, the wind data is filtered using a low pass Butterworth in time with a cut off period of 30 h to get only the background wind without changes due to gravity or tidal waves. The wind structure is shown in Figure 8 in an altitude range from the ground to 60 km. As ECMWF data have a sponge layer at ∼50 km, the reliability of the data decreases above this altitude. In general, the zonal and meridional winds show large temporal variations mainly in the upper troposphere.

While zonal winds at the altitude of about 10 km are weak and towards the East in the first days, the wind veers to the West on the 7 May for about 3 days. After this time an even stronger zonal wind towards the East is reestablished with wind velocities up to 18 m/s. At the same time a wind reversal in the meridional wind occurs. This wind component is blowing to the South in the first days. On 7 May the wind veers to the North until the end of 9 May. The wind reversal in the zonal and meridional component at the end of 9 May coincides with an increase of gravity wave activity and a disappearance of the diurnal tidal

Atmos. Chem. Phys. Discuss., https://doi.org/10.5194/acp-2017-537
Manuscript under review for journal Atmos. Chem. Phys.
Discussion started: 15 June 2017
© Author(s) 2017. CC BY 4.0 License.

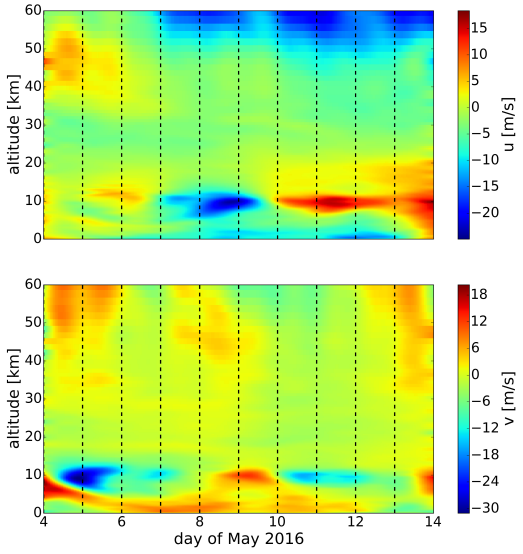

Figure 8. Zonal and meridional wind above Kühlungsborn on 4 - 13 May 2016 derived from ECMWF. The data has been low pass filtered with a cut off period of 30 h.

component after this point in time. We will examine the relation between gravity waves and the background wind further in Section 6.

Above 15 km altitude the zonal wind is generally weak. Between 15 and 20 km the wind direction is mostly towards the East in the last days. Above this altitude range the wind is blowing most of the time towards the West. At an altitude between 40 and 50 km the wind is slowly decreasing from eastward wind to weak westward wind. However, the overall weak variation of the horizontal wind above the tropopause is presumably caused by planetary waves.

We have also studied the ozone distribution provided by ECMWF as the excitation of solar tides is related to the absorption of solar radiation by ozone in the stratosphere in addition to water vapor in the troposphere. In Figure 9 the temporal evolution of the ozone concentration is shown up to an altitude of 60 km. The maximum of the ozone layer is located at an altitude of about 22 km with additional strong layers between 12 and 18 km. In the lower stratosphere the ozone shows a larger variability with a maximum on the 9 May. Above the maximum of the ozone layer, the ozone concentration decreases rapidly. However, we found no correlation between the time interval of the increasing ozone and the occurrence of the diurnal component. A closer look on parts of the ozone layer reveals a similar behavior of the ozone in an altitude range of 30-40 km as the diurnal component at ∼50 km altitude in the lidar data, but the relative change of the ozone is only 2%. It seems to be unlikely that these small ozone variations are the reason for a changing excitation of the diurnal tide during the sounding period. This is even more reliable, if we have a look on the much larger differences in the ozone below 30 km, which are clearly not correlated

Atmos. Chem. Phys. Discuss., https://doi.org/10.5194/acp-2017-537
Manuscript under review for journal Atmos. Chem. Phys.
Discussion started: 15 June 2017
© Author(s) 2017. CC BY 4.0 License.

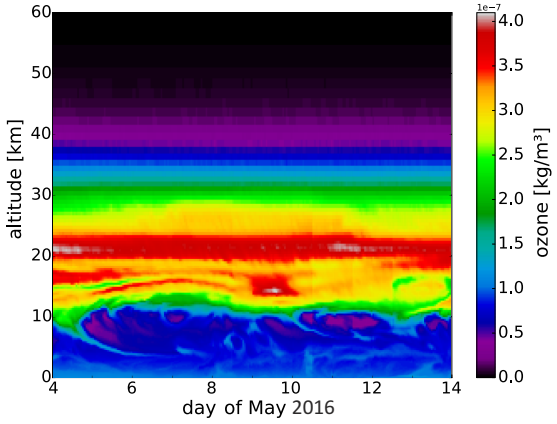

Figure 9. Ozone density from the ground to 60 km altitude above Kühlungsborn on 4 - 13 May 2016 derived from ECMWF

with the appearance of the diurnal tide. In general, a local change in the ozone layer is not expected as an relevant reason for a change in the tidal wave field.

6 Discussion

The daylight capability of the RMR lidar at Kühlungsborn allows us to study temperatures in the middle atmosphere during night and day and evan for a few consecutive days depending on cloud free conditions. During May 2016 an exceptional measurement lasting 10 days was performed at our site. Most other multi-day lidar studies are done with resonance lidars in an altitude range of 80-110 km because technologies for daylight suppression are available since many years for these type of lidars (e.g., States and Gardner, 2000; Fricke-Begemann and Höffner, 2005; Yuan et al., 2010; Cai et al., 2017). Another 3-day study for the middle atmosphere was performed by Baumgarten et al. (2015) also using an RMR lidar but at high latitudes. They investigated inertia gravity waves in temperature data with combined wind measurements.

Our unprecedented measurement reveals a strong variation of different atmospheric waves, especially around the stratopause. Between an altitude of 40 and 50 km the diurnal tidal wave component shows an increase as expected due to the decreasing air density. But surprisingly this increase is not visible during the whole time. Above 50 km the diurnal tidal wave component strongly decreases again. A nearly identical behavior of this tidal component is revealed using a composite analysis as an independent calculation method to determine a mean tidal amplitude. The appearance of the diurnal wave component in a particular altitude range is frequently related to a trapped mode of the tide, which can not propagate upward. Such a local maximum of the diurnal tide has also been reported by e.g. Forbes and Wu (2006) and Gan et al. (2014). However, results on the temporal variability are generally rare. To find possible reasons for the variability of the tidal component in our observations, ECMWF data from wind and ozone are investigated (shown in Figure 8 and 9). The ozone presumably leads to the excitation of the diurnal tide in the stratosphere as expected from theoretical studies (Forbes, 1995). But an ozone change is not the reason for

Atmos. Chem. Phys. Discuss., https://doi.org/10.5194/acp-2017-537
Manuscript under review for journal Atmos. Chem. Phys.
Discussion started: 15 June 2017
© Author(s) 2017. CC BY 4.0 License.

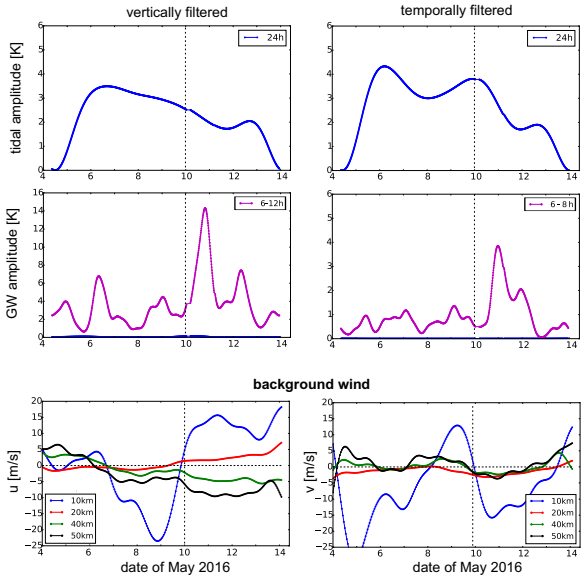

Figure 10. Wavelet amplitudes of the diurnal tide (at the top) and gravity waves (in the middle) at 45 km altitude compared to the zonal and meridional wind (at the bottom) from ECMWF at different altitudes. The vertical dashed line indicates 0 UT on 10 May.

the disappearance of the diurnal tide in the last days of the sounding because of two indications. First, the ozone concentration shows only small variations of ∼2% over the time between 30 and 40 km altitude compared to the huge amplitude variation of the diurnal tide of ∼50%. And second, the amplitude of the diurnal component is constant over the time at 40 km altitude, which is related to a constant excitation of this tide.

The strong correlation of the temporal evolution of the amplitudes of tidal and gravity waves and the winds suggests that there is a close connection between each other. This topic is highlighted in Figure 10 for an altitude of 45 km. Atmospheric waves propagate within the mean flow. The consequence of this is a possible Doppler-shift of the real intrinsic period, this shift of the period is observed by a ground-based instrument. To take this into account we summed up all amplitudes from waves with periods between 6 and 12 h (6 and 8 h) for further analysis to form a group of gravity waves for the vertically (temporally) filtered data, respectively. This is done under the estimation that a shift of the period is small as the horizontal wind components illustrate only small changes above the tropopause with time. Unfortunately, we do not know the propagation direction of the waves, which would be necessary to calculate the intrinsic wave periods from the observed ones. As already seen in the wavelet analysis there is a strong diurnal component, which reaches an amplitude of up to 4 K on 6 May at 12 UT. Later on, the amplitude is slowly decreasing for the vertically as well as the temporally filtered data. The minimum of this wave component is reached on 11 May for both filtering methods and the amplitudes are reduced by a factor of 2. Compared to this, the amplitudes of gravity waves are strongly increased on 10/11 May. The absolute value of the amplitudes are overestimated due to the integration across a range of periods, but nevertheless the increase is significant at this time, when the diurnal wave component is weak. The amplitude of the zonal and meridional background wind is also shown at different altitudes in Figure

© Author(s) 2017. CC BY 4.0 License.

10. The weakening of the diurnal wave component does not coincide with the wind reversal in the tropopause region. But it is reliable that after this wind reversal the gravity waves become important, especially those with periods <8 h. This indicates a difference for the vertical propagation conditions for these waves. Exactly such a behavior was already observed in the seasonal variation of these certain waves during summer in the study by Baumgarten et al. (2017). In this time these waves can propagate to higher altitudes compared to inertia gravity waves. The direction of the mean winds below 30 km altitude is typically towards the East during summer. This leads to a filtering of most of the waves except these with a high phase velocity towards the East.

In the next part of the discussion we want to demonstrate that the decrease of the diurnal tidal wave component is correlated with an increase of the gravity waves from the temporally filtered data and not with inertia gravity waves. We estimate this because the gravity waves from the temporally filtered data appear only in a limited altitude range of 42 to 52 km just in the same altitude region where the diurnal tide decreases (see Figure 11). Contrary to this, the inertia gravity waves show also a strong occurrence in the first days of the measurement and at lower altitudes (partly visible in Figure 6 on the left hand side), when also the diurnal tidal wave is strongly present. The strongest occurrence of gravity waves with periods <8 h is slightly before the the diurnal tidal wave component reaches its minimum. To demonstrate that this is closely linked, the altitude dependencies of the amplitudes of the diurnal tide as well as of gravity waves from the temporally filtered data are shown in Figure 11 for two certain times, namely when the minimum of the tide is reached and when the maximum of the GW occurs. For this analysis both types of waves are differently treated. While the maximal amplitude of the GW along the altitude is normalized to one, the minimal amplitude of the diurnal tide is also set in relation to the maximum of the tide on 6 May before a normalization along the altitude is done. This means, in each altitude the maximum of the tide is normalized to one, and the minimum values on the 11 May are stored. After this a normalization along the altitude is done as for the gravity waves. For the tidal amplitudes it has to be taken into account, that the amplitudes change over the whole time, therefore we have to relate the minimum to the overall temporal change of the tide. The result shows an occurrence of the gravity waves just between 42 and 52 km. Within this altitude range the amplitude of the diurnal tide starts to decrease. When the gravity waves disappear also the decrease of the amplitude of the diurnal tide stops. This behavior is probably related to an interaction between the gravity waves and the diurnal tide resulting in a suppression of the diurnal tide for several hours. This measurement provides an elegant demonstration of the strong impact of gravity waves on the diurnal tide. This is compatible with investigations by Ribstein et al. (2015). They have demonstrated a strong impact of GW on a slowly varying background, as it is caused by tides, and vice versa using model data. Most other weather and climate model studies are using simplifications which lead to overestimated amplitudes of GW in the mesosphere and thermosphere, which also lead to discrepancies for tidal amplitudes (Alexander et al., 2010; Senf and Achatz, 2011).

A closer look to the observations shown here reveals that the disappearance of the diurnal wave starts even before the gravity waves become prominent. We estimate that this is related to a stronger Doppler-shift of gravity waves to an observed period of 24 h in the first days of the sounding period. If this gravity waves have large vertical wavelengths and these large periods, they would contribute to the results for tides. This would explain that the composite analysis shows smaller amplitudes for the tidal components than the wavelet analysis. Furthermore the wind shows changes from weak eastward wind to westward wind in this altitude range above 40 km, which could lead to the Doppler-shift mentioned above. But in the end, we can not prove this

Atmos. Chem. Phys. Discuss., https://doi.org/10.5194/acp-2017-537
Manuscript under review for journal Atmos. Chem. Phys.
Discussion started: 15 June 2017
© Author(s) 2017. CC BY 4.0 License.

Atmospheric Chemistry and Physics Discussions

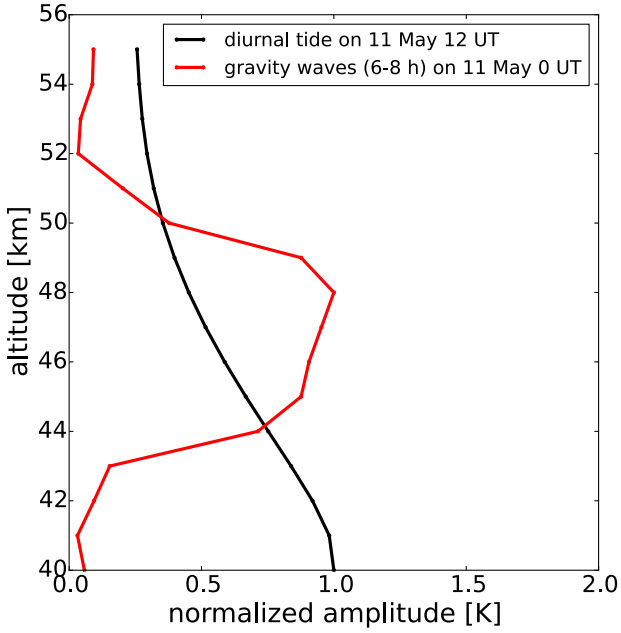

Figure 11. Wavelet amplitudes of the diurnal tide and of the gravity waves from the temporally filtered data on 11 May at 12 UT (0 UT) as a function of altitude.

because of missing modeling data with sufficient resolution and accuracy in this altitude range. Nevertheless, this study does indicate a wave-wave interaction of gravity waves and the diurnal tide.

7 Conclusions

In 2016 an unprecedented time series of temperature observations by lidar of about 10 days in the middle atmosphere at mid-latitudes showed a large temporal variability of tidal waves. Especially the amplitudes of the diurnal wave decreased during the last half of the sounding period. This means tides are highly variable even on periods of a few days. This needs to be taken into account when the sampling of tides occurs rather sporadic, e.g. by satellites. Basically due to different wind conditions during the measurement time in the tropopause there was a change in the propagation conditions for gravity waves. We conclude that this leads to the observed wave-wave interaction mainly between tides and GW with periods smaller than 8 h and therefore a disappearance of the tidal component in the last days of the measurement in an altitude range of 42-52 km. Both types of waves decrease above the stratopause region, which could be related to a destructive interference of these waves in addition to a trapped mode of the tide. Such a behavior is not well reproduced in model studies. The results of the study shown here highlight the necessity for a more sophisticated parametrization of GW in climate models. Therefore, the data set provides a possible benchmark for future comparisons with models.

Atmos. Chem. Phys. Discuss., https://doi.org/10.5194/acp-2017-537
Manuscript under review for journal Atmos. Chem. Phys.
Discussion started: 15 June 2017
© Author(s) 2017. CC BY 4.0 License.

Acknowledgements. The data for this paper are available upon request. We gratefully acknowledge Maren Kopp for her help in the installation of the daylight capable RMR lidar as well as Josef Höffner for his contribution to the beam stabilization. We thank Michael Priester and Torsten Köpnick for the maintenance of the RMR lidar system at IAP. We also acknowledge all our students for their numerous hours of lidar operation. This project was partly supported by the Deutsche Forschungsgemeinschaft (DFG, German Research Foundation) under project SPP1788 (DynamicEarth) - CH1482/1-1 (DYNAMITE) and under project LU1174/8-1 (PACOG), FOR1898 (MS-GWaves). The work was also partly supported by the Bundesministerium für Bildung und Forschung (BMBF, Federal Ministry of Education and Research) under project D/553/67210010 (ROMIC-GWLcycle).

© Author(s) 2017. CC BY 4.0 License.

References

Achatz, U., Grieger, N., and Schmidt, H.: Mechanisms controlling the diurnal solar tide: Analysis using a GCM and a linear model, Journal of Geophysical Research: Space Physics, 113, n/a–n/a, doi:10.1029/2007JA012967, http://dx.doi.org/10.1029/2007JA012967, a08303, 2008.

Alexander, M. J., Geller, M., McLandress, C., Polavarapu, S., Preusse, P., Sassi, F., Sato, K., Eckermann, S., Ern, M., Hertzog, A., Kawatani, Y., Pulido, M., Shaw, T. A., Sigmond, M., Vincent, R., and Watanabe, S.: Recent developments in gravity-wave effects in climate models and the global distribution of gravity-wave momentum flux from observations and models, Q. J. R. Meteorol. Soc., 136, 1103–1124, doi:10.1002/qj.637, http://dx.doi.org/10.1002/qj.637, 2010.

Baumgarten, G., Fiedler, J., Hildebrand, J., and Lübken, F.-J.: Inertia gravity wave in the stratosphere and mesosphere observed by Doppler wind and temperature lidar, Geophys. Res. Lett., 42, 10, 929–10, 936, doi:10.1002/2015GL066991, 2015.

Baumgarten, K., Gerding, M., and Lübken, F.-J.: Seasonal variation of gravity wave parameters using different filter methods with daylight lidar measurements at mid-latitudes, J. Geophys. Res.: Atmos., 122, 2683–2695, doi:10.1002/2016JD025916, 2017.

Cai, X., Yuan, T., and Liu, H.-L.: Large-scale gravity wave perturbations in the mesopause region above Northern Hemisphere midlatitudes during autumnal equinox: a joint study by the USU Na lidar and Whole Atmosphere Community Climate Model, Annales Geophysicae, 35, 181–188, doi:10.5194/angeo-35-181-2017, http://www.ann-geophys.net/35/181/2017/, 2017.

Chapman, S. and Lindzen, R. S.: Atmospheric tides: Thermal and Gravitational, Gordon and Breach New York, 1970.

Chu, X., Yu, Z., Gardner, C. S., Chen, C., and Fong, W.: Lidar observations of neutral Fe layers and fast gravity waves in the thermosphere (110–155 km) at McMurdo (77.8°S, 166.7°E), Antarctica, Geophys. Res. Lett., 38, n/a–n/a, doi:10.1029/2011GL050016, http://dx.doi.org/10.1029/2011GL050016, l23807, 2011.

Eckermann, S. D. and Marks, C. J.: An idealized ray model of gravity wave-tidal interactions, J. Geophys. Res.: Atmos., 101, 21 195–21 212, doi:10.1029/96JD01660, http://dx.doi.org/10.1029/96JD01660, 1996.

Eixmann, R., Gerding, M., Höffner, J., and Kopp, M.: Lidars with narrow FOV for spectral and daylight measurements, IEEE Transactions on Geoscience and Remote Sensing, 53, 4548–4553, doi:10.1109/TGRS.2015.2401333, 2015.

Fleming, E. L., Chandra, S., Barnett, J. J., and Corney, M.: Zonal mean temperature, pressure, zonal wind, and geopotential height as functions of latitude, Adv. Space Res., 10, 11–59, 1990.

Forbes, J. M.: Middle atmosphere tides, J. Atm. Terr. Phys., 46, 1049–1067, 1984.

Forbes, J. M.: Tidal and Planetary Waves, pp. 67–87, American Geophysical Union, doi:10.1029/GM087p0067, http://dx.doi.org/10.1029/GM087p0067, 1995.

Forbes, J. M. and Wu, D.: Solar Tides as Revealed by Measurements of Mesosphere Temperature by the MLS Experiment on UARS, J. Atmos. Sci., 63, 1776–1797, doi:10.1175/JAS3724.1, http://dx.doi.org/10.1175/JAS3724.1, 2006.

Fricke-Begemann, C. and Höffner, J.: Temperature tides and waves near the mesopause from lidar observations at two latitudes, Journal of Geophysical Research: Atmospheres, 110, n/a–n/a, doi:10.1029/2005JD005770, http://dx.doi.org/10.1029/2005JD005770, d19103, 2005.

Fritts, D. C. and Alexander, M. J.: Gravity wave dynamics and effects in the middle atmosphere, Reviews of Geophysics, 41, n/a–n/a, doi:10.1029/2001RG000106, 1003, 2003.

Gan, Q., Du, J., Ward, W. E., Beagley, S. R., Fomichev, V. I., and Zhang, S.: Climatology of the diurnal tides from eCMAM30 (1979 to 2010) and its comparison with SABER, Earth, Planets and Space, 66, 103, doi:10.1186/1880-5981-66-103, http://dx.doi.org/10.1186/1880-5981-66-103, 2014.

© Author(s) 2017. CC BY 4.0 License.

Gardner, C. S. and Voelz, D. G.: Lidar studies of the nighttime sodium layer over Urbana, Illinois: 2. Gravity waves, J. Geophys. Res.: Space Physics, 92, 4673–4694, doi:10.1029/JA092iA05p04673, http://dx.doi.org/10.1029/JA092iA05p04673, 1987.

Geller, M. A., Alexander, M. J., Love, P. T., Bacmeister, J., Ern, M., Hertzog, A., Manzini, E., Preusse, P., Sato, K., Scaife, A. A., and Zhou, T.: A Comparison between Gravity Wave Momentum Fluxes in Observations and Climate Models, Journal of Climate, 26, 6383–6405, doi:10.1175/JCLI-D-12-00545.1, http://dx.doi.org/10.1175/JCLI-D-12-00545.1, 2013.

Gerding, M., Kopp, M., Hoffmann, Höffner, J., and Lübken, F.-J.: Diurnal variation of midlatitude NLC parameters observed by daylight-capable lidar and their relation to ambient parameters, Geophys. Res. Lett., 40, 6390–6394, doi:10.1002/2013GL057955, 2013.

Gerding, M., Baumgarten, K., Höffner, J., and Lübken, F.-J.: Lidar Soundings between 30 and 100 km altitude during day and night for observation of temperatures, gravity waves and tides, EPJ Web of Conferences, 119, 13 001, doi:10.1051/epjconf/201611913001, http://dx.doi.org/10.1051/epjconf/201611913001, 2015.

Gerding, M., Kopp, M., Höffner, J., Baumgarten, K., and Lübken, F.-J.: Mesospheric temperature soundings with the new, daylight-capable IAP RMR lidar, Atmos. Meas. Tech., 9, 3707–3715, doi:10.5194/amt-9-3707-2016, 2016.

Gille, J., Barnett, J., Arter, P., Barker, M., Bernath, P., Boone, C., Cavanaugh, C., Chow, J., Coffey, M., Craft, J., Craig, C., Dials, M., Dean, V., Eden, T., Edwards, D. P., Francis, G., Halvorson, C., Harvey, L., Hepplewhite, C., Khosravi, R., Kinnison, D., Krinsky, C., Lambert, A., Lee, H., Lyjak, L., Loh, J., Mankin, W., Massie, S., McInerney, J., Moorhouse, J., Nardi, B., Packman, D., Randall, C., Reburn, J., Rudolf, W., Schwartz, M., Serafin, J., Stone, K., Torpy, B., Walker, K., Waterfall, A., Watkins, R., Whitney, J., Woodard, D., and Young, G.: High Resolution Dynamics Limb Sounder: Experiment overview, recovery, and validation of initial temperature data, Journal of Geophysical Research: Atmospheres, 113, n/a–n/a, doi:10.1029/2007JD008824, http://dx.doi.org/10.1029/2007JD008824, d16S43, 2008.

Hauchecorne, A. and Chanin, M. L.: Density and Temperature Profiles obtained by Lidar between 35 and 70 km, Geophys. Res. Lett., 7, 565–568, 1980.

Hertzog, A., Boccara, G., Vincent, R. A., Vial, F., and Cocquerez, P.: Estimation of Gravity Wave Momentum Flux and Phase Speeds from Quasi-Lagrangian Stratospheric Balloon Flights. Part II: Results from the Vorcore Campaign in Antarctica, Journal of the Atmospheric Sciences, 65, 3056–3070, doi:10.1175/2008JAS2710.1, http://dx.doi.org/10.1175/2008JAS2710.1, 2008.

Hoffmann, P., Becker, E., Singer, W., and Placke, M.: Seasonal variation of mesospheric waves at northern middle and high latitudes, J. Atmos. Sol. Terr. Phys., 72, 1068–1079, doi:10.1016/j.jastp.2010.07.002, 2010.

Holton, J. R. and Alexander, M. J.: The Role of Waves in the Transport Circulation of the Middle Atmosphere, pp. 21–35, American Geophysical Union, doi:10.1029/GM123p0021, http://dx.doi.org/10.1029/GM123p0021, 2000.

Kim, Y., Eckermann, S. D., and Chun, H.: An overview of the past, present and future of gravity-wave drag parametrization for numerical climate and weather prediction models, Atmosphere-Ocean, 41, 65–98, doi:10.3137/ao.410105, http://dx.doi.org/10.3137/ao.410105, 2003.

Kopp, M., Gerding, M., Höffner, J., and Lübken, F.-J.: Tidal signatures in temperatures derived from daylight lidar soundings above Kühlungsborn (54°N, 12°E), J. Atmos. Sol. Terr. Phys., pp. 37–50, doi:10.1016/j.jastp.2014.09.002, 2015.

Preusse, P., Eckermann, S. D., and Ern, M.: Transparency of the atmosphere to short horizontal wavelength gravity waves, J. Geophys. Res.: Atmos., 113, n/a–n/a, doi:10.1029/2007JD009682, http://dx.doi.org/10.1029/2007JD009682, d24104, 2008.

Ribstein, B., Achatz, U., and Senf, F.: The interaction between gravity waves and solar tides: Results from 4-D ray tracing coupled to a linear tidal model, J. Geophys. Res.: Space Phys., 120, 6795–6817, doi:10.1002/2015JA021349, http://dx.doi.org/10.1002/2015JA021349, 2015JA021349, 2015.

© Author(s) 2017. CC BY 4.0 License.

Sakazaki, T., Fujiwara, M., Zhang, X., Hagan, M. E., and Forbes, J. M.: Diurnal tides from the troposphere to the lower mesosphere as deduced from TIMED/SABER satellite data and six global reanalysis data sets, J. Geophys. Res.: Atmos., 117, n/a–n/a, doi:10.1029/2011JD017117, http://dx.doi.org/10.1029/2011JD017117, d13108, 2012.

Senf, F. and Achatz, U.: On the impact of middle-atmosphere thermal tides on the propagation and dissipation of gravity waves, J. Geophys. Res.: Atmos., 116, n/a–n/a, doi:10.1029/2011JD015794, http://dx.doi.org/10.1029/2011JD015794, d24110, 2011.

States, R. J. and Gardner, C. S.: Thermal Structure of the Mesopause Region (80-105 km) at 40° N Latitude. Part II: Diurnal Variations, Journal of the Atmospheric Sciences, 57, 78–92, doi:10.1175/1520-0469(2000)057<0078:TSOTMR>2.0.CO;2, http://dx.doi.org/10.1175/1520-0469(2000)057<0078:TSOTMR>2.0.CO;2, 2000.

VanZandt, T. E.: A universal spectrum of buoyancy waves in the atmosphere, Geophys. Res. Lett., 9, 575–578, doi:10.1029/GL009i005p00575, http://dx.doi.org/10.1029/GL009i005p00575, 1982.

Wilson, R., Chanin, M. L., and Hauchecorne, A.: Gravity waves in the middle atmosphere observed by Rayleigh lidar: 1. Case studies, J. Geophys. Res.: Atmos., 96, 5153–5167, doi:10.1029/90JD02231, http://dx.doi.org/10.1029/90JD02231, 1991.

Yuan, T., She, C.-Y., Krueger, D., Reising, S. C., Zhang, X., and Forbes, J. M.: A collaborative study on temperature diurnal tide in the midlatitude mesopause region (41° N, 105° W) with Na lidar and TIMED/SABER observations, J. Atmos. Sol. Terr. Phys., 72, 541 – 549, doi:http://dx.doi.org/10.1016/j.jastp.2010.02.007, http://www.sciencedirect.com/science/article/pii/S1364682610000556, 2010.